Characterisation of growth & structure of TCNQ phases on Ag(111)

P.J. Blowey[1,2], A. Haags[3,4], L.A. Rochford[5], J. Felter[3,4], D.A. Warr[6], D.A. Duncan[2], T.-L. Lee[2], G. Costantini[6], C. Kumpf [3,4], D.P. Woodruff [1*]

(1) Physics Department, University of Warwick, Coventry CV4 7AL, UK
(2) Diamond Light Source, Harwell Science and Innovation Campus, Didcot, OX11 0DE, UK
(3) Peter Grünberg Institut (PGI-3), Forschungszentrum Jülich, 52425 Jülich, Germany
(4) Jülich-Aachen Research Alliance (JARA) – Fundamentals of Future Information Technology, 52425 Jülich, Germany
(5) Chemistry Department, University of Birmingham, University Road, Birmingham B15 2TT, UK
(6) Chemistry Department, University of Warwick, Coventry CV4 7AL, UK

Abstract

A combination of scanning tunnelling microscopy (STM), low energy electron diffraction (LEED) and low energy electron microscopy (LEEM) has been used to identify the structural phases formed by 7,7,8,8-tetracyanoquinodimethane (TCNQ) on Ag(111). These comprise a 2-D gas phase, a low density commensurate (LDC) phase and a higher density incommensurate (HDI) phase. LEEM also shows the presence of an additional 'precursor-HDI' phase with a surface unit mesh area only ~3% less than the HDI phase. Normal incidence X-ray standing wave (NIXSW) measurements of the HDI phase yield almost identical structural parameters to the LDC phase for which a full structure determination was been previously reported. The results show TCNQ does not adopt the inverted bowl distortion favoured in earlier density functional theory calculations of TCNQ on coinage metal surfaces, but the N atoms are twisted out of the molecular plane, an effect found for the LDC phase to be due to incorporation of Ag adatoms. The possible role of Ag adatoms in the HDI phase, and in the transition from the precursor-HDI phase, is discussed.

* to whom all correspondence should be addressed: D.P.Woodruff@warwick.ac.uk

I. INTRODUCTION

The increasing maturity of surface science techniques over the last decade or two has led to detailed investigations of increasingly complex adsorption systems and the resulting interfaces. These have progressed through simple atomic adsorbates and diatomic molecules, relevant to inorganic semiconductor interfaces and simple catalytic reactions, to significantly larger molecules including those relevant to organic electronics. The electronic properties of metal-organic interfaces have a profound influence on the functionality of resulting devices, most obviously influenced by the energy alignment of the metal Fermi level and the highest occupied and lowest unoccupied (HOMO and LUMO) molecular orbitals of the organic molecules. Surface science studies of the earliest stages of formation of model interfaces can play an important role in gaining a better understanding of their properties. These investigations of extremely well-characterised idealised model systems cannot be expected to have short-term direct impact on practical device design, but offer a route to understanding the underlying physics that determines the intermolecular and molecule-substrate ordering and interactions. Nevertheless, most such studies are conducted on molecules that have some relevance to molecular electronics, although the specific molecule/substrate interfaces accessible to these surface science methods are not directly relevant to practical electronic devices. One molecule of this type that has attracted significant interest is 7,7,8,8-tetracyanoquinodimethane (TCNQ), which is a strong electron acceptor capable of forming highly conducting charge transfer salts in combination with suitable electron donor molecules. However, despite a significant number of surface science investigations of TCNQ/metal interfaces in the last few years, there has been a dearth of quantitative structural studies, and based on the widely-accepted axiom that ‘structure determines function’, our work has focussed on these missing structural studies.

As an isolated molecule TCNQ (Fig. 1) has a rigid planar structure but, following uptake of electrons, the central quinoid ring aromatises, disrupting the conjugated π-system that extends through the whole neutral molecule, making the molecule far more flexible. Evidence from experimental studies, particularly using X-ray photoelectron spectroscopy

(XPS), has indicated that this electron transfer occurs on a number of coinage metal surfaces, and density functional theory (DFT) calculations have predicted that the resulting flexible molecule bends into an inverted bowl configuration with the N atoms as much as 1.4 Å below the central quinoid ring [1, 2, 3, 4, 5, 6, 7].

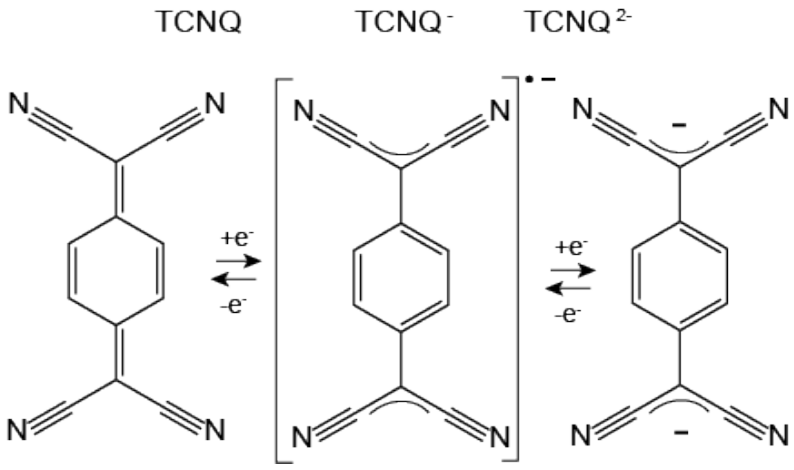

Fig. 1 The chemical structure of TCNQ and the influence of electron addition to the molecule.

However, with the exception of some near-edge X-ray absorption spectroscopy (NEXAFS) for TCNQ adsorbed on Cu(100) [**Error! Bookmark not defined.**], which indicates tilting of the C-N bonds relative to the surface plane (but not whether the tilt is up or down), there is no experimental evidence to support this conclusion. By contrast, very recently we have completed a quantitative experimental structural investigation of a commensurate $\begin{pmatrix} 2 & 5 \\ -8 & -2 \end{pmatrix}$ phase of TCNQ adsorbed on Ag(111) using normal incidence X-ray standing waves (NIXSW) [8] and showed that the molecule does *not* adopt this bent configuration in this phase [9]. Through comparison of the NIXSW data with dispersion-corrected DFT calculations we concluded that instead the adsorbed molecule twists such that some C-N are tilted out of the surface to bond to Ag adatoms, while other C-N bonds tilt down to bond to the Ag atoms in the underlying surface.

In this paper we report the details of the formation of both this commensurate phase and a second incommensurate phase developing at a higher molecular density of TCNQ on Ag(111). We identify these phases by scanning tunnelling microscopy (STM) and low energy electron diffraction (LEED), and follow the growth and transformations between

these phases by low energy electron microscopy (LEEM) [10, 11]. We also report on the results of NIXSW measurements of the incommensurate phase and discuss their possible interpretation.

2. EXPERIMENTAL DETAILS

Detailed characterisation of the TCNQ adsorption phases formed by vacuum deposition onto a clean Ag(111) surface at room temperature was undertaken by STM and low-current (micro-channel plate) MCP-LEED in an ultra-high vacuum (UHV) chamber at the University of Warwick, by low-current MCP-LEED, soft X-ray photoelectron spectroscopy (SXPS) and NIXSW in the UHV end-station installed on beamline I09 of the Diamond Light Source (DLS) electron storage ring, and by LEEM and μLEED in an Elmitec AC-SPE-LEEM III instrument at Forschungszentrum Jülich. At Warwick and DLS the single crystal Ag(111) substrate (cutting precision of 0.1°) was prepared *in situ* using cycles of sputtering with 1 keV Ar^+ ions for 30 minutes followed by annealing to ~500 °C for 30 minutes. At Jülich sputtering cycles involved two periods of 20 minutes at different incident angles, followed by annealing in steps of 1 K/s up to 700°C. A clean well-ordered sample was obtained as judged by LEED and STM at Warwick, by LEEM and μLEED at Jülich and by LEED and SXPS at Diamond. LEED patterns obtained at all three sites provided a clear reference of the preparation of the same TCNQ adsorption phases (under closely similar preparation conditions) for the complementary experiments. All STM images in this work were analysed, plane corrected and flattened using the Gwyddion open-source software [12]. The high-resolution soft XP spectra and the XP spectra recorded in NIXSW experiments were fitted using the CasaXPS software package. The programs FIJI [13] and LEEDcal [14, 15] were used for image correction of the LEEM and μLEED data collected at Jülich.

3. SURFACE CHARACTERISATION

Deposition of TCNQ onto the Ag(111) surface led to the identification of the two ordered overlayer phases described in the introduction. Fig. 2 shows typical STM images and LEED patterns collected in Warwick. The identified matrices of the unit meshes used to

produce the LEED simulations were $\begin{pmatrix} 2 & 5 \\ -8 & -2 \end{pmatrix}$ for the commensurate phase (Figs. 2a, b, c) and $\begin{pmatrix} 0.93 & 4.26 \\ -2.91 & -1.63 \end{pmatrix}$ for the incommensurate phase (Figs. 2d, e, f).

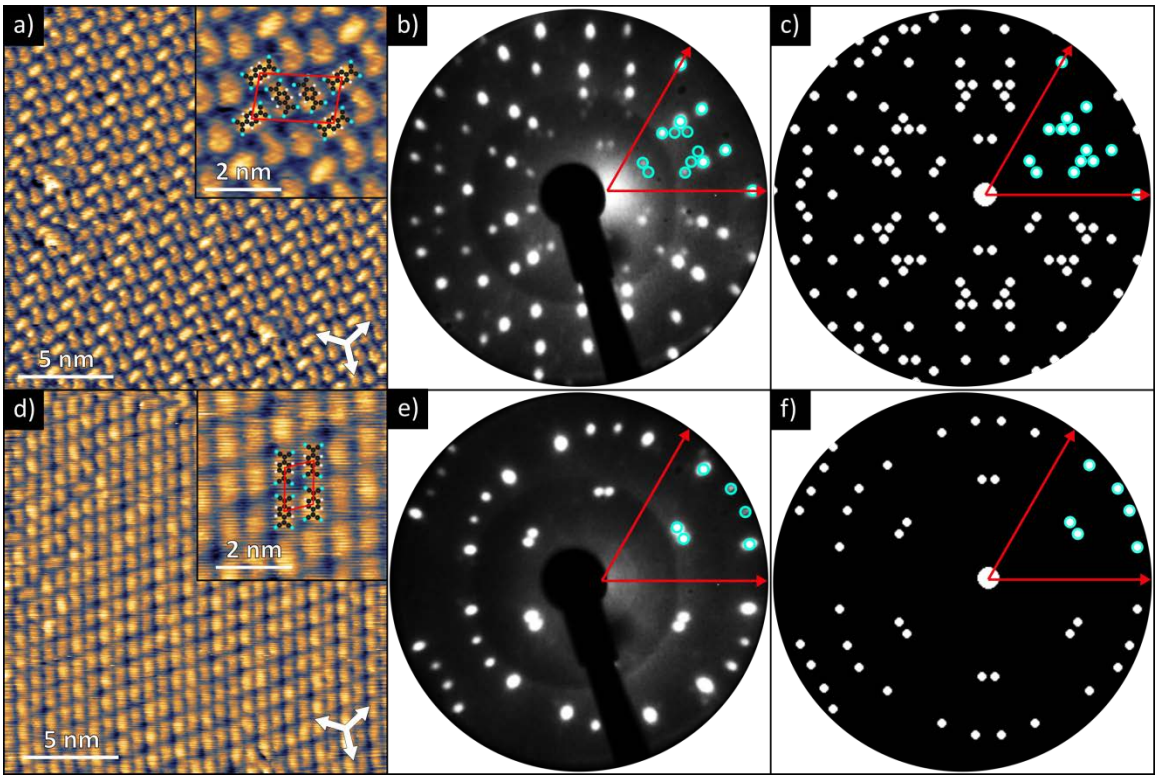

Fig. 2. STM and LEED images from the commensurate (a, b, c) and incommensurate (d, e, f) ordered phases of TCNQ on Ag(111). (a) and (d) show STM images (with enlarged insets including superimposed molecular models of the TCNQ molecules represented in the images). (b) and (e) show LEED patterns recorded at 14.5 eV electron energy, while (c) and (f) show simulated LEED patterns based on the identified unit meshes using the LEEDpat program [16]. The superimposed circles on the experimental patterns in (b) and (e) highlight diffracted beam locations for one sector of the pattern predicted by the simulations. STM operating conditions were (a) V_{samp} = -1.0 V, I = 55 pA (b) V_{samp} = 0.25 V, I = 85 pA).

These matrices, used in the simulations to give a good fit to the experimental LEED patterns, correspond to unit mesh dimensions of 12.6 Å by 20.8 Å with an included angle of 97.3°, which corresponds to an area of 259 $Å^2$ for the commensurate mesh and 11.2 Å by 7.3 Å with an included angle of 106.0° implying an area of 78.4 $Å^2$ for the incommensurate phase. The STM images indicate that each unit mesh of the commensurate phase contains three molecules, whereas the unit mesh of the incommensurate phase contains only a single molecule.

Using the traditional definition of 1 ML as equal to the number of Ag atoms within each Ag(111) atomic layer leads to molecular coverages of these two phases as 0.086 ML (LDC) and 0.091 ML (HCI). However, to avoid confusion between these *local* coverages and the *average* coverage particularly relevant to the LEEM investigation of the formation of these phases, we hereafter refer to the *local* coverage as *density* and will refer to the *average coverage* as simply *coverage*. The incommensurate phase has a 6% higher molecular density than the commensurate phase, so these two phases will be referred to hereafter as LDC (lower-density commensurate) and HDI (higher-density incommensurate).

As indicated in the introduction, a full structure determination of the LDC phase has already been published [9]. The only previously reported observations of the HDI phase appear to be in the paper of Wäckerlin *et al.* [17], who presented an STM image that shows a similar ordering of molecular features, and in a later PhD thesis [18].

Deposition of a high coverage of TCNQ at room temperature commonly led to the appearance of a LEED pattern consistent with the coexistence of the two identified ordered phases. Brief annealing of these mixed phase surfaces typically led to a pure HDI phase (at ~210°C) that transformed into a pure LDC phase at ~270°C. Corresponding SXP spectra also indicated that this phase transition was accompanied by a small decrease in coverage. High resolution C 1s and N 1s SXP spectra also show relative photoelectron binding energies characteristic of electron transfer to the adsorbed TCNQ in both phases [17, 19, 20, 21] (see Fig. S1 in Supplemental Material [22]). This is

consistent with work function changes relative to the clean surface obtained from the cut-off voltage in ultraviolet photoemission measurements (+0.43±0.14 eV for the LDC phase and +0.54±0.14 eV for the HDI phase) and from the LEEM-IV measurements (+0.50±0.05 eV for the LDC phase and +0.60±0.05 eV for the HDI phase). While the static LEED, SXPS and STM measurements provide a wealth of information on the lateral structure and coverage of the TCNQ phases, they provide little insight towards the dynamics of how these layers form and, as will be seen in the following, the presence of disordered and transient phases. For this insight, we must turn to the LEEM measurements.

4. LEEM STUDY OF THE TCNQ ADSORPTION PHASES

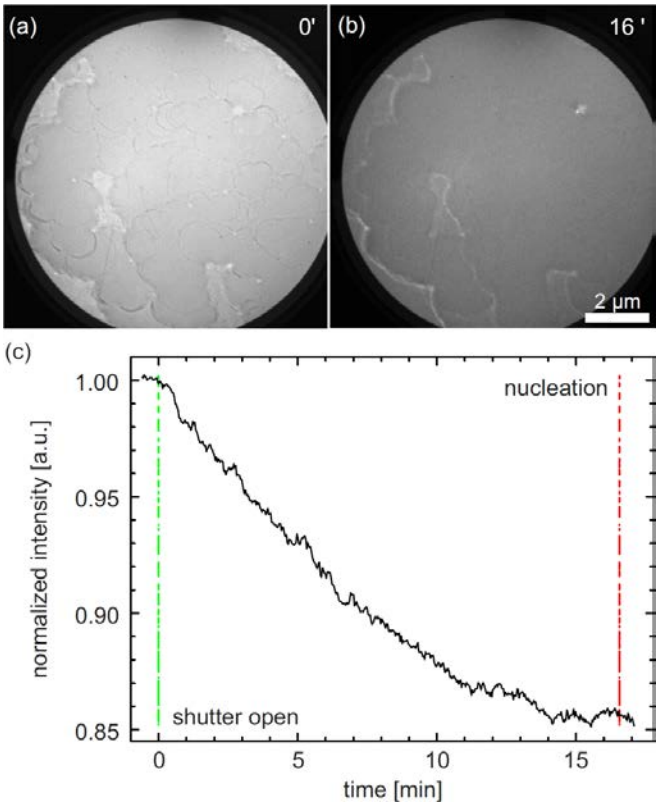

Fig. 3: (a,b) LEEM images taken during the deposition of TCNQ on the Ag(111) surface (U_{start} = 2 V[†], underfocus conditions, field of view: 10 µm): (a) at t = 0 (clean Ag(111) surface), (b) at t = 16 min. In (b) the surface is covered by a disordered gas-like phase. (c) Normalised LEEM intensity plotted vs. time during the deposition of TCNQ. The green and red lines mark the times when TCNQ deposition started and when the nucleation of islands began, respectively.

[†] In LEEM the "start voltage" is the common designation for the kinetic energy at which the electrons interact with the sample surface. The high energy electrons coming from the illumination column of the microscope are decelerated down to the 'start energy' by an electrostatic field between the objective lens and the sample surface. After interacting with the sample the electrons are reaccelerated by the same field, before they enter the imaging electron optics. Small values of this electron energy at the sample (below 5 eV) are often used for sensitive samples in order to avoid radiation damage.

The LEEM technique [10, 11] allows one to follow *in situ* and in real time the nucleation, growth and phase transitions of an adsorbate layer on a surface, and the surface unit mesh, of individual regions down to sub-micrometer sizes using the μLEED capability. In addition, however, it also provides qualitative information on changes to the surface that do not correspond to ordered overlayers.

This is illustrated by the results in Fig. 3, which shows LEEM images from (a) the clean Ag(111) surface and (b) after a TCNQ deposition time of 16 minutes with the sample at room temperature, together with (c) a plot of the overall LEEM intensity throughout this deposition period. Both LEEM images show only some weak features due to monoatomic step edges and bunches of step edges, as well as some defects. Throughout this period μLEED showed no overlayer-derived diffraction beams. However Fig. 3(c) demonstrates clearly that the overall image brightness decreases throughout this deposition period, which must be attributed to an increasing coverage of adsorbed TCNQ in a 2D gas phase. At a deposition time of 16min 30sec, marked by the red line in Fig. 3(c), small islands begin to nucleate on the surface.

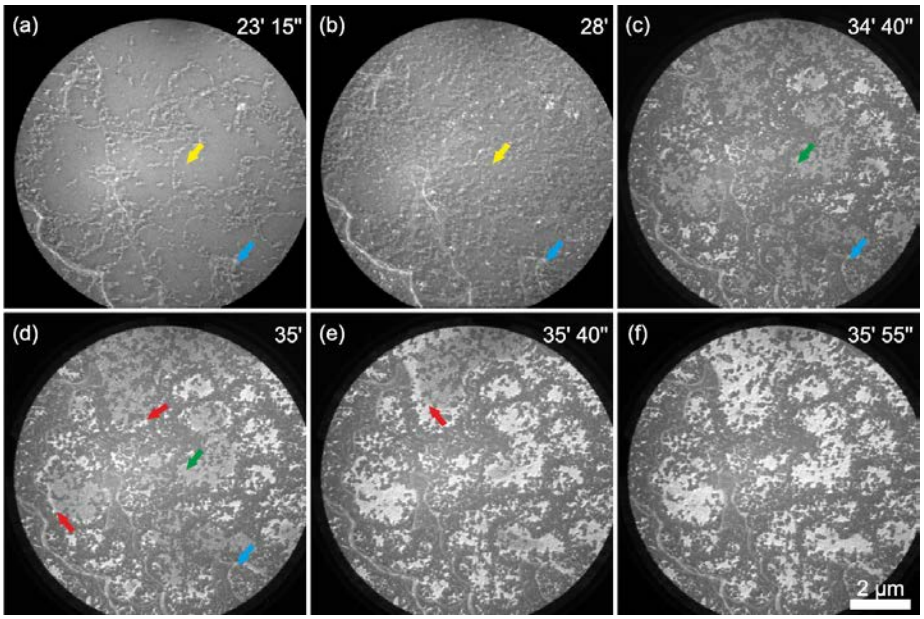

Fig. 4: LEEM images (U_{start} = 2 V, underfocus conditions) taken after nucleation of TCNQ islands on the Ag(111) surface. The corresponding deposition times are given in minutes (') and seconds ('') in the images. The scale bar is valid for all panels. The coloured arrows identify examples of different phase regions: yellow 2D gas, blue LDC, green precursor-HDI, red HDI (see text). The full movie is available as ESM.

The LEEM image series is continued in Fig. 4 for deposition times from 23 to 36 min, with nucleated islands (examples identified by blue arrows) being clearly seen in (a) after a total TCNQ deposition time of 23min 15sec. These islands appear slightly brighter than the 2D gas phase (yellow arrows), and are identified in μLEED as LDC phase islands (blue arrows). Please note that the full deposition movie (covering the time sequence from which Fig. 3a,b and Fig. 4 are extracted) is available in several versions as electronic supplemental material [22]. Upon further TCNQ deposition, the LDC islands grow in size while retaining their level of brightness. The initial 2D gas phase, however, fully disappears and is replaced by a phase that appears even brighter than the LDC phase, see green arrows in Fig. 4 (c). This latter phase is a previously unidentified "precursor" to the HDI phase, with a distinct μLEED pattern, as discussed more fully below. In our experiments the precursor-HDI phase was rather unstable and transformed to the HDI phase within approximately 1 min (see Fig. 4c-f). This transition was seen to occur with a sharp reaction front starting at the edges of the precursor-HDI islands and running through the islands towards their centre (marked by red arrows in Fig. 4d and e). The clear difference in brightness in the LEEM images between the precursor-HDI and the HDI islands implies that these areas do correspond to two distinct structural phases. We further note that while the transition does not start simultaneously for all precursor islands, within each island the velocity of the reaction front is rather uniform and seems not to depend on the island size. After 36 minutes of total deposition time (see Fig. 4f) the transformation is complete and the LEEM images exhibit only two different brightness levels, corresponding to the HDI phase after the discussed transition, and the small, unaffected LDC islands. μLEED measurements unambiguously confirmed the structures of the islands and the assignment of them with the corresponding brightness in LEEM (LDC appears darker than HDI, see Fig. 4f). The diffraction patterns are identical to those found in the Warwick and Diamond experiments (Fig. 2b and e). We would like to mention that the coexistence of the LDC and HDI phases, as shown in Fig. 4(f), was usually observed for a saturated TCNQ layer formed at room temperature.

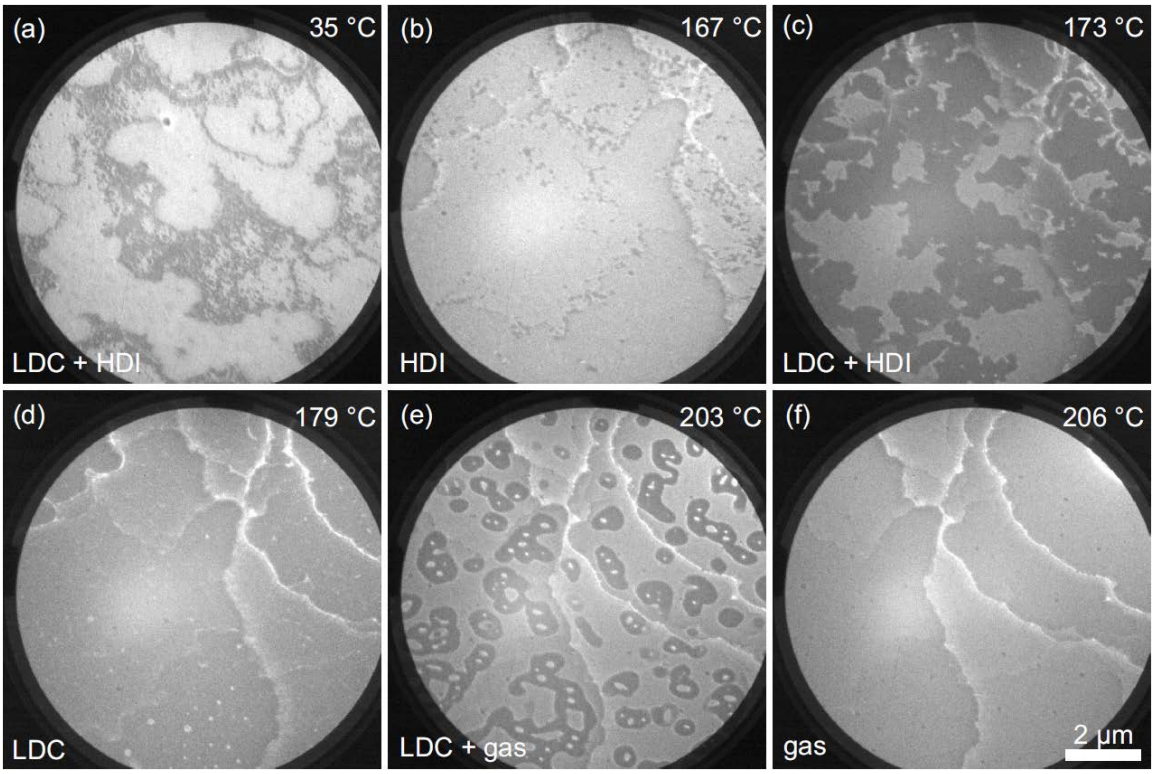

Fig. 5. Sequence of LEEM images (U_{start}=1.3 V, slight underfocus)recorded during annealing a TCNQ/Ag(111) monolayer. (a) coexisting LDC (dark) and HDI (bright) islands. (b) After annealing to 167°C, the HDI phase becomes dominant and is (in a small temperature window) the only stable phase. (c,d) Above 173°C the HDI phase gradually (re)transforms into the LDC phase that is homogeneously covering the surface at 179°C. (e,f) Above 200°C the LDC layer breaks up and is gradually replaced by a 2D gas phase. The full movie is available as electronic Supplemental Material [22]

Further TCNQ deposition did not lead to any further growth of either phase or additional brightness changes that might be expected if a second layer of TCNQ is formed. A relatively small sticking coefficient of second layer molecules at room temperature might account for this. However, we cannot exclude the possibility that some second layer molecules are present in a 2D gas phase similar to the first layer at low coverages. The presence of some second layer molecules might explain the observation that mild annealing of a sample on which the LDC and HDI phases coexist leads to the disappearance of the LDC phase and the formation of a homogeneous monolayer of the (higher density) HDI phase, as can be seen in Fig. 5(a,b): the darker LDC islands disappear upon annealing above 150°C and only the HDI phase is visible in Fig. 5(b). Annealing to higher temperatures leads to desorption of TCNQ molecules, initially

resulting in a transformation of the homogeneous HDI layer into an LDC overlayer (Fig. 5c and d), while annealing to higher temperatures (above 200°C, see Fig. 5 e) causes this homogeneous LDC layer to break up into individual LDC islands surrounded by 2D gas phase regions. These islands continuously shrink until the surface is covered only by the gas phase at temperatures above 205°C (Fig. 5f). Note that a full movie of these transitions is available as ESI. This behaviour on annealing is equivalent to that seen by STM and LEED in the experiments performed at Warwick, although the transition temperatures differ slightly, most probably due to different temperature calibrations.

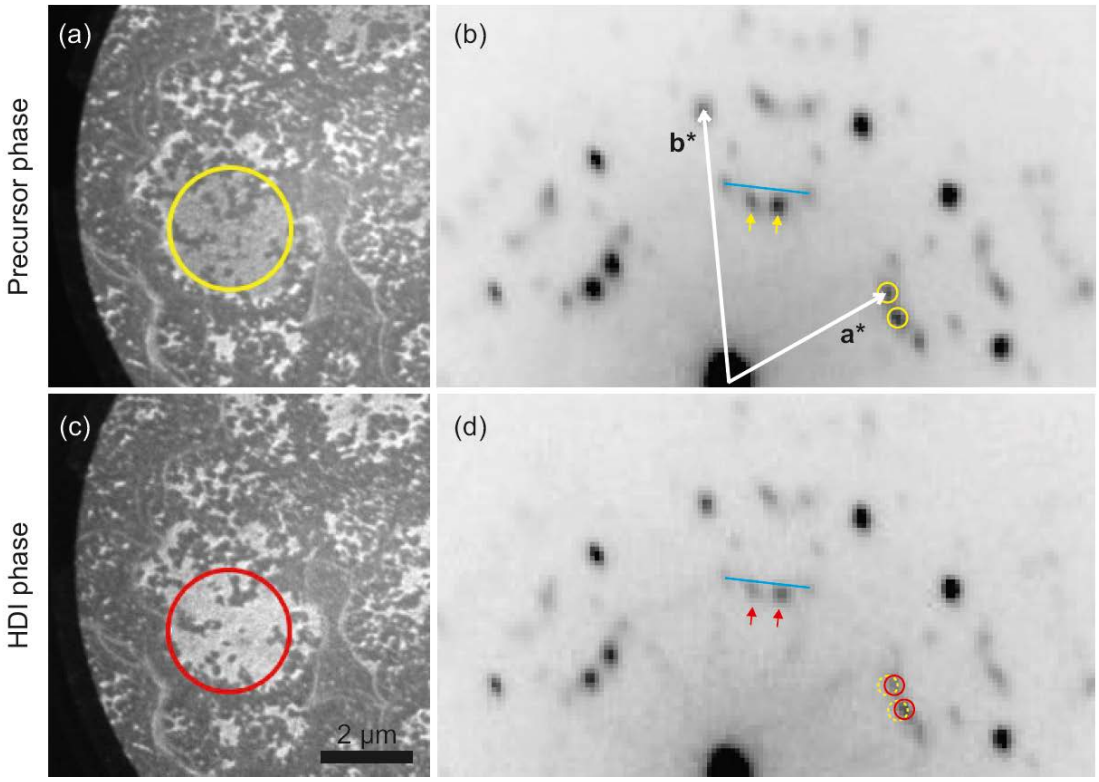

Fig 6: LEEM and µLEED images recorded for (a, b) the precursor-HDI phase and (c, d) the HDI phase. Yellow and red circles in the LEEM images indicate the selected surface area for the µLEED measurements. The primitive translation vectors of the reciprocal mesh of this phase, **a*** and **b***, are superimpoise in (b). The most obvious changes in the LEED patterns are indicated by yellow and red circles as well as by blue lines and yellow/red arrows in the LEED patterns, for details see text. (LEEM: U_{start} = 1.3 V, underfocus conditions, µLEED: U_{start} = 17 V).

Finally we discuss the structural difference between the precursor-HDI and the HDI phase based on µLEED measurements. Fig. 6 shows LEEM images and µLEED

diffraction patterns before (a, b) and after (c, d) the phase transition between these phases. The corresponding μLEED patterns show the difference between the two phases to be rather subtle. Only very small shifts of some of the LEED spots (marked by yellow and red circles in Figs. 6b and 6d) distinguish the two phases. In (d) these beams (red circles) have shifted radially outwards from the specular beam by a very small amount, relative to the locations of the same beams (yellow circles) in (b). This small displacement is more clearly visible by comparing the location of these beams relative to the LEED diffracted beams of small coexistent islands of the LDC phase that are present in the surface area selected for these μLEED measurements. Two of these LDC beams are connected by a blue line in Figs. 6b and 6d, which can be taken as reference for the positions of the precursor-HDI and HDI spots marked with yellow and red arrows. In (d) (HDI phase) these spots are clearly closer to the reference line than in (c) (precursor-HDI phase).

The small outward radial shift of the LEED beams indicates a slight lengthening of the surface reciprocal mesh primitive translation vector **a***, arising from a small expansion of the reciprocal unit mesh (**b*** appears to be unchanged). However, this effect is very small; it corresponds to a compression of approximately 3 % of the unit mesh area in real space. As such, the very significant observed difference in the LEEM brightness is rather surprising. This suggests that beside the small compression of the unit mesh, another more significant change in the geometric structure may be associated with the phase transition. For example, there could be a change in the adsorption height, or in the tilt angle, of the adsorbed molecules, which could lead to a change in the LEED intensity-energy (I-V) spectrum and therefore to a significant change in the observed LEEM intensity. An alternative possibility is some modification in the underlying Ag(111) surface geometry, by the addition or removal of Ag adatoms (identified as an ingredient of the LDC structure [9] and previously speculated to occur in the HDI phase [17]) or by a change in the surface corrugation. In view of the much higher atomic number of the Ag atoms, and of the consequential larger scattering cross-section, rearrangement of these atoms may be a more likely cause of the change in the LEEM intensity (and in the entire LEEM-I-V curve).

5. NIXSW RESULTS

The NIXSW technique, with the X-ray absorption monitored by the resulting core level photoemission signal, provides a method of determining the height above a surface of the atoms within an element-specific and chemical-state-specific fashion [8]. A detailed structural analysis of the LDC phase, based on a combination of NIXSW data and the results of DFT calculations has already been published [9]. A similar DFT simulation of the HDI phase is not possible because these calculations rely on having a commensurate molecular superstructure. However, NIXSW can be applied to such a system and a comparison of the NIXSW results for the two phases provides some insight into the structure of the HDI phase. Full details of the NIXSW measurement methodology and the treatment of the results, including taking account of non-dipolar modification of the photoelectron angular distributions, are provided in Ref. [9]. Analysis of the experimental data leads to the extraction of two structural parameters, the coherent position p and the coherent fraction, f. Each atomic species that can be distinguished by their photoelectron binding energies, namely the N atoms, the C atoms bonded to the N atoms, the C atoms bonded only to other C atoms and the C atoms bonded to H atoms; each will have a corresponding p and f value that is unique to its adsorption height(s). The coherent fraction is generally considered as an order parameter, with perfect order (static and dynamic) corresponding to a value of unity. In practice, a value of greater than ~0.80 is generally regarded as representative of all the contributing atoms occupying a single height given by the coherent position; much lower values usually indicate multiple height contributions. The coherent position is a measure of the height above the nearest extended bulk lattice atomic scattering plane in units of the bulk interlayer spacing, $d_{(111)}$. It is related to the true height D by $D = (p+n)d_{(111)}$, where n is the number of extended scattering planes located between the surface and the adsorbate. This integer is generally easily selected by ensuring that the resulting interatomic distances are physically reasonable. Table I summarises the structural parameter values obtained from the NIXSW measurements, the coherent position values being expressed as D values in ångström units with $n = 1$. The corresponding experimental data for the HDI phase, and their fits, are shown in Fig. S2 in the supplemental material [22], also compared with the experimental data for the LDC phase and their fits [9].

	f		*D* (Å)	
Component	LDC [9]	HDI	LDC [9]	HDI
CH	0.95(10)	1.04(10)	2.86(5)	2.83(5)
CC	0.99(10)	1.02(10)	2.78(5)	2.77(5)
CN	0.89(10)	0.94(10)	2.76(5)	2.74(5)
N	0.39(10)	0.41(10)	2.75(5)	2.67(5)

Table I Summary of the NIXSW structural parameters obtained for the two different ordered phases of TCNQ on Ag(111). Error estimates for each value are shown in parentheses in units of 0.01. Coherent fraction values are uncorrected for a detector nonlinearity [19] that can give rise to anomalous values slightly greater than unity, covered by the relative large error estimates of ±0.10.

All parameter values are very similar for the two different structural phases. The coherent fractions for all the C atoms are indicative of well-defined single heights, while the associated coherent positions indicate a barely significant buckling of the planar structure of the free molecule. For both phases, however, the coherent fraction for the N atoms is too low to be reconciled with a single height. For the LDC phase this result led to the exploration, using DFT, of a structural model including Ag adatoms that provided excellent agreement with the NIXSW parameter values [9]. Specifically, the low *f* value for the N atoms can be assigned to them occupying two different heights, the lower one corresponding to N atoms bonded to the underlying Ag substrate atoms while the higher one is associated with N atoms bonding to Ag adatoms. Figure S3 in the Supplemental Material [22] illustrates, using an Argand diagram representation of the NIXSW parameters of Table I, how two different N atom heights can account for the low coherent fraction and the general kind of molecular conformation that this implies.

A detailed structure determination of the HDI phase is not possible because an equivalent DFT calculation cannot be used to model the incommensurate phase. However, the NIXSW results clearly show that the adsorbed TCNQ in this phase does not adopt the

inverted bowl distortion that has been predicted in many earlier DFT calculations of TCNQ adsorbed on coinage metal surfaces; specifically, the carbon atoms retain an essentially planar geometry while the N atoms show almost the same *average* height but must be significantly bent out of plane both towards and away from the surface. This strong similarity to the LDC phase clearly raises the possibility that the presence of Ag adatoms could also account for the low N coherent fraction in the HDI phase. The presence of adatoms in this structure was tentatively proposed by Wäckerlin *et al.* [17], based on the qualitative appearance of a mixture of bright and dark spots in between the TCNQ molecules in their STM images. They interpreted the bright spots as Ag atoms and the dark spots as vacancies, though they detected a high degree of mobility of these features, which may be surprising as it would imply rapid diffusion of Ag adatoms within a 2D metal-organic framework. Our own STM images of this phase (Fig. 2d) show some features similar to the dark regions reported by Wäckerlin *et al*, but not the bright spots. Notice that in the case of the LDC phase we have previously shown that the absence of features in STM images associated with Ag adatoms is consistent with DFT-based simulations of these images [9].

6. CONCLUSIONS

A combination of STM, LEED and LEEM has identified two main ordered overlayer phases of TCNQ on Ag(111): a commensurate $\begin{pmatrix} 2 & 5 \\ -8 & -2 \end{pmatrix}$ (LDC) phase with a lower molecular density and an incommensurate $\begin{pmatrix} 0.93 & 4.26 \\ -2.91 & -1.63 \end{pmatrix}$ (HDI) phase, with a ~6% higher local molecular coverage (density). This qualitative behaviour is similar to that found for NTCDA on the same surface, the phases equivalent to HDI and LDC in this case being referred to as ‘compressed monolayer’ and ‘relaxed monolayer’ [23]. LEEM results show clearly the progression of the surface phases with increasing coverage from a two-dimensional gas phase, the nucleation of the LDC phase and transformation to the HDI phase, but with an additional precursor-HDI phase also being formed prior to HDI. μLEED shows the unit meshes of these two HDI phases to differ very slightly, with a

compression of the area of the surface mesh from the precursor phase to the HDI phase of only ~3%.

NIXSW measurements of the two main phases yield very closely similar structural parameter values. In particular, in both phases the average heights, above the surface, of all the constituent atoms of the TCNQ molecule are very similar, clearly showing the molecule does not adopt the inverted (or any sort of) bowl shape as has been predicted for adsorption on several coinage metal surfaces. However, the NIXSW coherent fraction for the N atoms clearly indicates an out-of-plane distortion of the molecule with N atoms having displacements of opposite sign out of this plane. The previous report [9] of the LDC phase, combining both NIXSW measurements and dispersion-corrected DFT calculations, showed that these results can be reconciled with a structural model involving incorporation of Ag adatoms into the molecular adsorption layer. Because the HDI phase is incommensurate, no comparable DFT calculations are possible, but the strong similarity of the NIXSW parameter values for the LDC and HDI phases does seem to imply that Ag adatoms are also likely to be a component of this structure. What is less clear is the nature of the structural differences that distinguish the HDI phase and its precursor. Despite the very small difference in the unit mesh of these structures, the intensity of the (bright field) LEEM images of these two island phases is significantly different, implying a difference in the LEED (00) beam I-V characteristics. This is most readily reconciled with a difference in the two structures perpendicular to the surface. One possible origin of this could be associated with a different reorganisation of Ag adatoms in these two structural phases.

Acknowledgements

The authors thank Diamond Light Source for access to beamline I09 (proposal number SI12975) that contributed to the results presented here. P.J.B. acknowledges financial support from Diamond Light Source and EPSRC. J.F. and C.K. acknowledge financial support by the Deutsche Forschungsgemeinschaft (DFG) through the Collaborative Research Centre SFB 1083.

References

1 D. Stradi, B. Borca, S. Barja, M. Garnica, C. Diaz, J. M. Rodriguez-Garcia, M. Alcami, A. L. Vazquez de Parga, R. Miranda and F. Martin, RSC Adv., **6**, 15071 (2016).

2 L. Romaner, G. Heimel, J.-L. Brédas, A. Gerlach, F. Schreiber, R. L. Johnson, J. Zegenhagen, S. Duhm, N. Koch and E. Zojer, Phys. Rev. Lett., **99**, 256801 (2007).

3 T.-C. Tseng, C. Urban, Y. Wang, R. Otero, S. L. Tait, M. Alcamí, D. Écija, M. Trelka, J. M. Gallego, N. Lin, M. Konuma, U. Starke, A. Nefedov, A. Langner, C. Wöll, M. Á. Herranz, F. Martín, N. Martín, K. Kern and R. Miranda, Nat. Chem., **2**, 374 (2010).

4 S. Barja, D. Stradi, B. Borca, M. Garnica, C. Díaz, J. M. Rodriguez-García, M. Alcamí, A. L. V. de Parga, F. Martín and R. Miranda, J. Phys. Condens. Matter, **25**, 484007 (2013).

5 J. I. Martínez, E. Abad, F. Flores and J. Ortega, Phys. Status Solidi B, **248**, 2044 (2011).

6 M. N. Faraggi, N. Jiang, N. Gonzalez-Lakunza, A. Langner, S. Stepanow, K. Kern and A. Arnau, J. Phys. Chem. C, **116**, 24558 (2012).

7 A. Della Pia, M. Riello, D. Stassen, T.S. Jones, D. Bonifazi, A. De Vita and G. Costantini, Nanoscale, **8**, 19004 (2016).

8 D.P. Woodruff , Rep. Prog. Phys. 68, 743 (2005).

9 P.J. Blowey, S. Velari, L.A. Rochford, D.A. Duncan, D.A. Warr, T.-L. Lee, A. De Vita, G. Costantini, and D.P. Woodruff, Nanoscale **10**, 14984 (2018).

10 E. Bauer, Rep. Prog. Phys. **57**, 895 (1994).

11 R.M. Tromp, IBM J. Res. Dev. **44**, 503 (2000).

12 D. Nečas and P. Klapetek, Cent. Eur. J. Phys., **10**, 181 (2012).

13 J. Schindelin, I. Arganda-Carreras, E. Frise, V. Kaynig, M. Longair, T. Pietzsch, S. Preibisch, C. Rueden, S. Saalfeld, B. Schmid, J. Y. Tinevez, D. J. White, V. Hartenstein, K. Eliceiri, P. ToFiji: An open-source platform for biological-image analysis. Nature Methods, **9**, 676, (2012).

14 F. Sojka, M. Meissner, C. Zwick, R. Forker,T. Fr itz.. Rev. Sci. Instrum., **84**, 15 (2013).

15 ScientaOmicron GmbH. https://www.scientaomicron.com/en/products/350/1155 Technical report. 15

16 K. E. Hermann and M. A. Van Hove, *LEEDpat (version 4.2)*, 2014, http://www.fhi-berlin.mpg.de/KHsoftware/LEEDpat/index.html.

17 C. Wäckerlin, C. Iacovita, D. Chylarecka, P. Fesser, T.A. Jung, N. Ballav, Chem. Commun. 47, 9146 (2011).

18 J. R. Fernandez, PhD thesis, Universidad Autónoma de Madrid, 2014.

19 P. J. Blowey, L. A. Rochford, D. A. Duncan, D. A. Warr, T.-L. Lee, D.P. Woodruff, and G. Costantini, Disc. Faraday. Soc, 204, 97 (2017).

20 R. Precht, R. Hausbrand and W. Jaegermann, Phys. Chem. Chem. Phys., 17, 6588 (2015).

21 R. Precht, S. Stolz, E. Mankel, T. Mayer, W. Jaegermann and R. Hausbrand, Phys. Chem. Chem. Phys., **18**, 3056 (2016).

22 See Supplemental Material at [URL] for SXP spectra, NIXSW data fits and LEEM movies.

23 A. Schöll, Y. Zou, T. Schmidt, R. Fink and E. Umbach, J. Phys. Chem. B **108**, 14741 (2004).